

MAGNETIC POWER SPECTRA DERIVED FROM GROUND AND SPACE MEASUREMENTS OF THE SOLAR MAGNETIC FIELDS

V. ABRAMENKO¹, V. YURCHYSHYN², H. WANG² and P. R. GOODE²

¹*Crimean Astrophysical Observatory, 98409, Nauchny, Crimea, Ukraine*
(e-mail: avi@crao.crimea.ua)

²*Big Bear Solar Observatory, 40386 N. Shore Lane, Big Bear City, CA 92314, USA*

(Received 15 December 2000; accepted 9 March 2001)

Abstract. We study magnetic power spectra of active and quiet regions by using Big Bear Solar Observatory and SOHO/MDI measurements of longitudinal magnetic fields. The MDI power spectra were corrected with Gaussian Modulation Transfer Function. We obtained reliable magnetic power spectra in the high wave numbers range, up to $k = 4.6 \text{ Mm}^{-1}$, which corresponds to a spatial scale $l = 1.4 \text{ Mm}$. We find that the occurrence of the spectral discontinuity at high wave numbers, $k \geq 3 \text{ Mm}^{-1}$, largely depends on the spatial resolution of the data and it appears at progressively higher wave numbers as the resolution of the data improves. The spectral discontinuity in the raw spectra is located at wave numbers about 3 times smaller than wave numbers, corresponding to the resolution of the data, and about 1.5–2.0 times smaller in the case of the noise- and-resolution corrected spectra. The magnetic power spectra for active and quiet regions are different: active-region power spectra are described as $\sim k^{-1.7}$, while in a quiet region the spectrum behaves as $\sim k^{-1.3}$. We suggest that the difference can be due to small-scale dynamo action in the quiet-Sun photosphere. Our estimations show that the dynamo can generate more than 6% of the observed magnetic power.

1. Introduction

Many phenomena in the solar atmosphere result from direct and continuous interaction of the magnetic fields with photospheric plasma flows, which are known to be turbulent. It has been shown that the supergranulation velocity field is responsible for the well-known web-like structure of the photospheric magnetic fields and the chromospheric network (Leighton, 1964; Simon and Leighton, 1964). This velocity field will move a given element of gas about in the photosphere, and will evidently act in the same way upon a magnetic line of force. If the magnetic field is organized into thin tubes, then its transport will be fully determined by the kinematics of the turbulent flows owing to the drag. To the contrary, in the case of thick flux bundles their transport will be dominated by dynamical forces like curvature forces, Coriolis force, etc. (see for details, Petrovay and Szakály, 1993). Transport of the small-scale magnetic fields in the photosphere is considered to be a passive response of the vertical component of the magnetic field to continual turbulent fluid motions (Nakagawa and Priest, 1973).

One way to explore the interaction between the magnetic fields and plasma motion is by investigating the nature of the photospheric magnetic fields in terms



of their magnetic power spectrum. The relevant description of turbulence can be only statistical because an individual study of some particular characteristic of fluid flow is impossible. Usually, theoretical magnetic power spectra, obtained under different physical assumptions, are compared with observational spectra in order to understand the underlying physics. The magnetic power spectrum reveals ongoing dynamics and represents the hierarchical distribution of the magnetic power at different spatial scales and can be described as $E(k) \sim k^\mu$, where $\mu < 0$ within some range of wave numbers called the inertial range (Monin and Yaglom, 1975). If, at all measurable scales, a spectrum shows the presence of the power that decreases within some range of scales, then one deals with turbulence and the power spectrum is associated with an energy cascade of turbulent motions. In the turbulent fluid motion, the kinetic energy cascades from small to large wave numbers, k , continuously converting the kinetic energy into the heat at large wave numbers. A steady-state turbulence, with spectral behavior of k^μ , is maintained when the rate of the kinetic energy supply is balanced by the rate of viscous dissipation. Spectral discontinuities, which divide the power spectrum into spectral sub-ranges may indicate the presence of different energy transfer mechanisms and/or energy input at certain spatial scales. Thus, the morphology of the magnetic power spectra is of vital importance for understanding the observed distribution of the photospheric magnetic fields and for elaborating of theoretical models of photospheric turbulence.

In constructing of the magnetic power spectrum a set of problems arises. First, one can only calculate a 2D instead of a 3D-spectrum, for we lack the required vertical resolution in the magnetic field measurements. Second, both instrumental noise and seeing affect the data, and thus their influence should be taken into account.

In the past, magnetic power spectra have been investigated in several studies (Nakagawa and Priest, 1973; Nakagawa and Levine, 1974; Knobloch and Rosner, 1981; Lee *et al.*, 1997). Nakagawa and Priest (1973) obtained spectra from longitudinal magnetograms of typical active and quiet regions with a spatial resolution of $2.5''$. Both the active-region and quiet-region spectra show spectral discontinuities at wave number $k^* = 0.63 \text{ Mm}^{-1}$, which corresponds to a spatial scale of 10 Mm. On wave numbers $k < k^*$ the active-region spectrum behaves as $\sim k^{-1}$, while the quiet-Sun spectrum is described by $k^{-0.3}$. Later, using high-resolution Big Bear videomagnetograms with a spatial resolution of $0.6''$, Lee *et al.* (1997) calculated the magnetic power spectrum for a quiet region. The spectrum was carefully corrected for noise and seeing. The authors report the presence of a spectral discontinuity at $k^* = 3.0 \text{ Mm}^{-1}$, which corresponds to a size of the largest granule – 2.1 Mm. At smaller wave numbers the spectra can be fitted by k^{-1} while at wave numbers higher than k^* the spectrum behaves as $\sim k^{-3.7}$. If the spectral discontinuity represented the intrinsic nature of the photospheric magnetic fields, indicating spatial scale, l^* , where the energy transfer regime changes, then its position in the spectrum should not depend on spatial resolution of the observational data.

In order to address the problem, we use here ground- and space-based measurements of the longitudinal magnetic fields. We obtain reliable magnetic power spectra at high wave numbers and study their structure.

2. Observations

Our data include the Big Bear Solar Observatory (BBSO) and SOHO/MDI measurements of the magnetic fields in active and quiet regions. Observations of AR NOAA 8375 were made on 4 November 1998, when the active region was located at the center of the solar disk. Figure 1(a) shows the BBSO longitudinal video-magnetogram obtained at 17:25 UT in the Ca I 6103 Å spectral line with a pixel size of $0.76'' \times 0.60''$. The SOHO/MDI magnetogram was recorded at 16:32 UT on 4 November 1998, with a pixel size of $0.6'' \times 0.6''$ in the Ni I 6767 Å spectral line (Figure 1(b)).

The BBSO magnetogram was carefully co-aligned with the MDI magnetogram and re-scaled. We also used magnetograms of two different quiet regions. The first one is the BBSO magnetogram recorded on 20 September 1998, at 16:52 UT near the center of the solar disk – far away from the active region magnetic fields. The magnetogram of size $390'' \times 300''$ is shown in Figure 2(a). Because the MDI magnetogram has a large field of view ($420'' \times 420''$), the second quiet-region magnetogram we used is a part of the MDI longitudinal magnetogram of size $350'' \times 150''$ just to the south of AR 8375 (Figure 2(b)).

3. Data Reduction and Calculation of Power Spectra

The energy spectrum of a 2D real function $u(\mathbf{l})$ is defined as (Monin and Yaglom, 1975)

$$F(\mathbf{k}) = |U(\mathbf{k})|^2, \quad (1)$$

where $U(\mathbf{k})$ is the Fourier transform of $u(\mathbf{l})$ and \mathbf{k} is a wave vector. In our case $u(\mathbf{l})$ is specified on a rectangular grid ω defined as

$$\omega : (x_i = i \Delta x, i = 1, \dots, N_x; y_j = j \Delta y, j = 1, \dots, N_y). \quad (2)$$

Then $U(\mathbf{k})$ are complex numbers on a grid Ω :

$$k_{x,i} = i \Delta k_x, i = -\left(\frac{N_x}{2} - 1\right), \dots, \frac{N_x}{2} \quad (3)$$

and

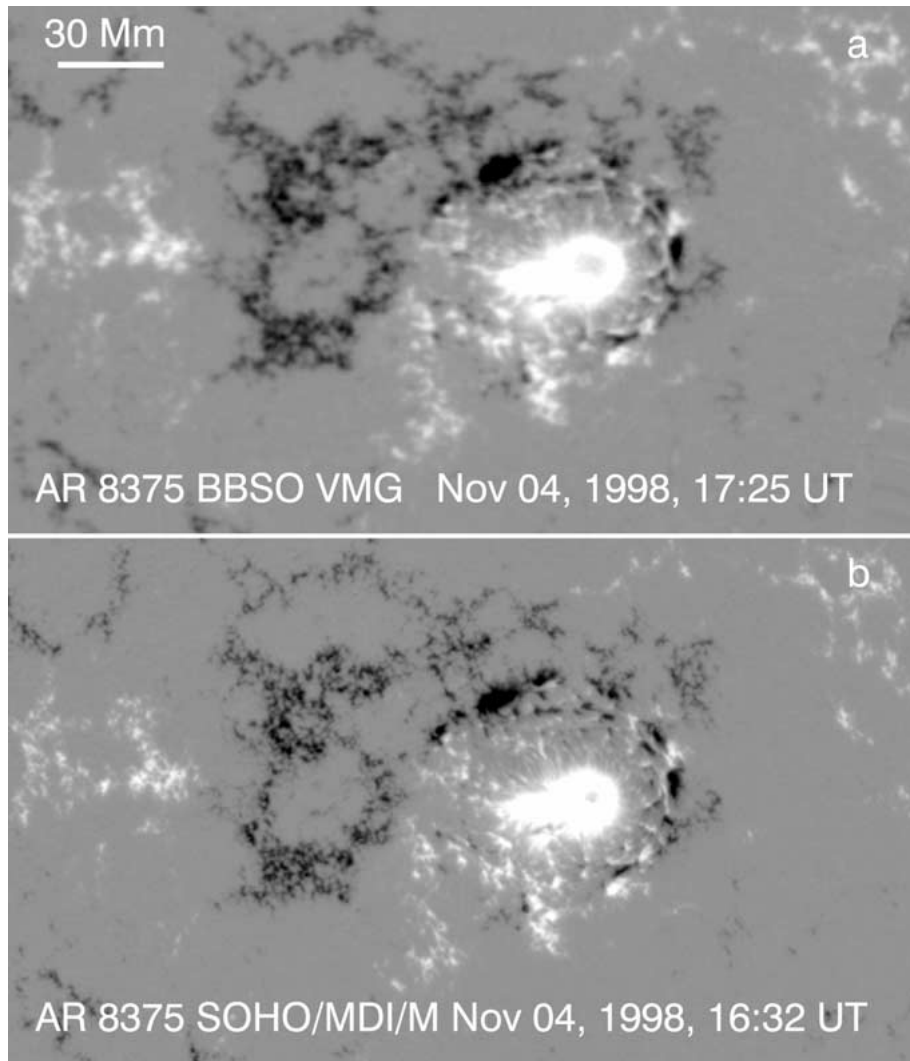


Figure 1. Maps of the longitudinal magnetic field of AR NOAA 8375. Magnetic fields of 750 G and stronger are shown in *white* (positive) and *black* (negative). (a) The measurements of the BBSO videomagnetograph system; (b) the SOHO/MDI magnetogram.

$$k_{y,j} = j \Delta k_y, j = -\left(\frac{N_y}{2} - 1\right), \dots, \frac{N_y}{2}, \quad (4)$$

where

$$\Delta k_x = 2\pi/(N_x \Delta x) \quad \text{and} \quad \Delta k_y = 2\pi/(N_y \Delta y). \quad (5)$$

From the Fourier Transform of function $u(\mathbf{l})$, we calculated function $F(\mathbf{k})$ using expression (1). We shifted $F(\mathbf{k})$ in k -space in order to obtain $F(\mathbf{k})$ on grid Ω with

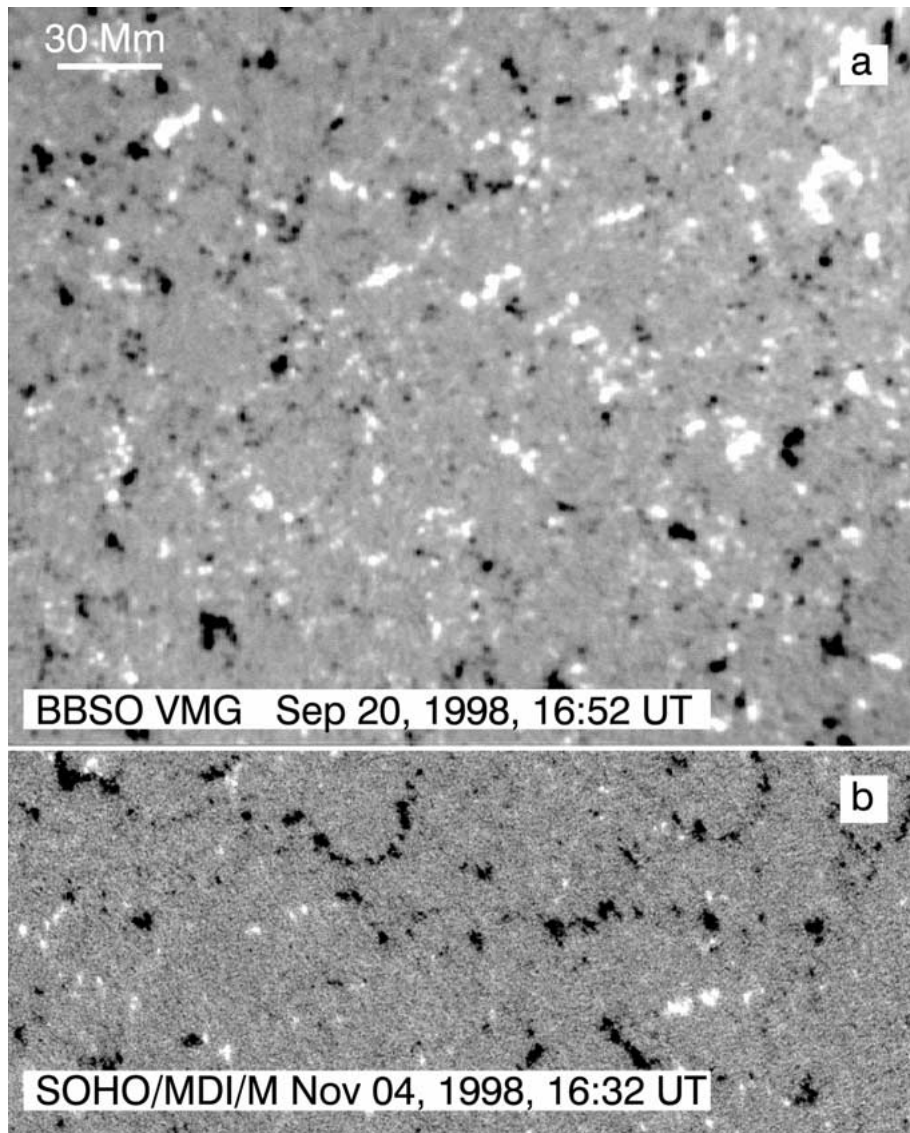


Figure 2. Maps of longitudinal magnetic fields in two different quiet regions. Magnetic fields of 50 G and stronger are shown in *white* (positive) and *black* (negative). (a) The measurements of the BBSO videomagnetograph system; (b) the SOHO/MDI magnetogram.

a zero frequency at the center of the coordinate system. It should be done in order to calculate power spectrum $E(k)$, where $k = \sqrt{k_x^2 + k_y^2}$. A power spectrum is defined as (Monin and Yaglom, 1975)

$$E(k) = \int_{|\mathbf{k}|=k} F(\mathbf{k}) dS(\mathbf{k}), \quad (6)$$

where $dS(\mathbf{k})$ is an element of the length of circle $|\mathbf{k}| = k$. Applying the mean value theorem to the integral (6) we can calculate $E(k)$ as follows:

$$E(k_m) = 2\pi k_m \sum_{k_m - (dk/2) \leq |\mathbf{k}| \leq k_m + (dk/2)} F(k_x, k_y) / N(k_m), \quad (7)$$

where the sum is taken over $N(k_m)$ nodal points inside the area of an annulus enclosed by two circles of radii $k_m - dk/2$ and $k_m + dk/2$. The width of the annulus is defined as

$$dk = n \sqrt{\Delta k_x^2 + \Delta k_y^2}, \quad (8)$$

where n is a real number. The width does not affect the slope of the calculated spectrum, however, it defines its quality and spectral resolution. If we assume n to be within the range $1 < n < 1.9$ then, being strongly jagged, the spectrum has efficient spectral resolution. To the contrary, when $n > 2.5$, the spectrum is smooth enough, but the spectral resolution suffers from a lack of points in the low wave number range of the spectra. When $n = 2$, it is a good compromise between the spectral resolution and quality of the spectrum. Because we specified Δx and Δy in expression (5) to be equal to the pixel size, measured in Mm, wave number k and linear scale l are related by expression l [Mm] = $2\pi/k$. Expression (6) was used to calculate magnetic power spectra for both active-region and quiet-Sun magnetic fields. Since the areas covered by each magnetogram differ considerably, all spectra were converted to normalized energy spectra by dividing an original spectrum by the area of the corresponding magnetogram.

In Figure 3 we show the magnetic power spectra calculated for the active region from the BBSO and MDI magnetograms. One sees that in the spectral range $0.16 < k < 1.4 \text{ Mm}^{-1}$ the spectra show fairly similar spectral behavior with the power-law index $\mu = -1.7$. However, the BBSO spectrum deviates from the dashed $\sim k^{-1.7}$ line at wave number $k = 1.4 \text{ Mm}^{-1}$, while the MDI spectrum turns off the line at wave number $k = 2.1 \text{ Mm}^{-1}$. Since they are the magnetic power spectra of the same active region, we assume that the difference is due to effect of the Earth's atmosphere on the ground-based measurements of the magnetic fields.

In order to avoid strong contributions to the power spectrum coming from the sunspot and the associated leakage of the magnetic power from low to high wave numbers, we blocked out the sunspot and recalculated the spectra. The 'spot corrected' BBSO spectrum is shown in Figure 6(a) with thick line. One sees that the major contribution from the sunspot comes on scales, $l > 9 \text{ Mm}$ (corresponding wave numbers are smaller than 0.7 Mm^{-1}), while the size of the sunspot was about 25 Mm . We next correct for noise and seeing only the 'spot-corrected' BBSO and MDI spectra, and we will limit the effective spectra up to scales insensitive to the presence of the sunspot, i.e., $l < 9 \text{ Mm}$.

At high wave numbers the spectra are flat, which indicates the presence of noise (Figures 3 and 6, $k > 5 \text{ Mm}^{-1}$). Under the assumption that the spectral power

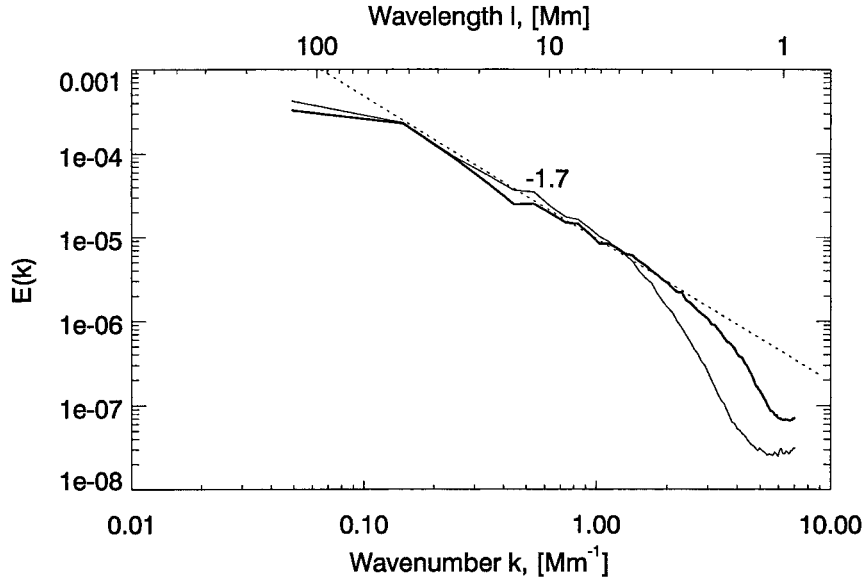


Figure 3. Raw active-region magnetic power spectra obtained from the BBSO (*thin line*) and the MDI (*thick line*) magnetograms. The *dashed line* shows best linear fit $\sim k^{-1.7}$ to both spectra.

of noise does not depend on the wave number, we subtract the power level of noise from the ‘spot-corrected’ spectra and plot them in Figure 6. The raw ‘spot-corrected’ spectra do not differ from the noise-corrected spectra (hereafter denoted as AR BBSO VMG and AR MDI/M) at small wave numbers $k < 3.5 \text{ Mm}^{-1}$, however, the later decreases faster at high wave numbers.

The next step was to reduce distortion of the AR MDI/M power spectra due to the finite spatial resolution of the MDI telescope. Using the diffraction limit of the telescope, $\theta = 1.25''$, we constructed Gaussian Modulation Transfer Function (MTF), which relates a raw spectrum $E(k)$ and an intrinsic power spectrum $\tilde{E}(k)$ (Margenau, 1964):

$$E(k) = \tilde{E}(k) |MTF|^2(k). \quad (9)$$

It is a challenging task to construct a precise MTF, however, in the case of MDI data the problem seems to be easier: there is no distortion of the data due to the Earth’s atmosphere and the pixel size is smaller than the diffractive limit of the telescope. Using Rayleigh criteria for the resolution limit

$$2h\left(\frac{\theta}{2}\right) = \frac{3}{4}h(0), \quad (10)$$

where $h(x)$ is Gaussian distribution function with standard deviation σ , we find a relation between σ and the resolution limit θ :

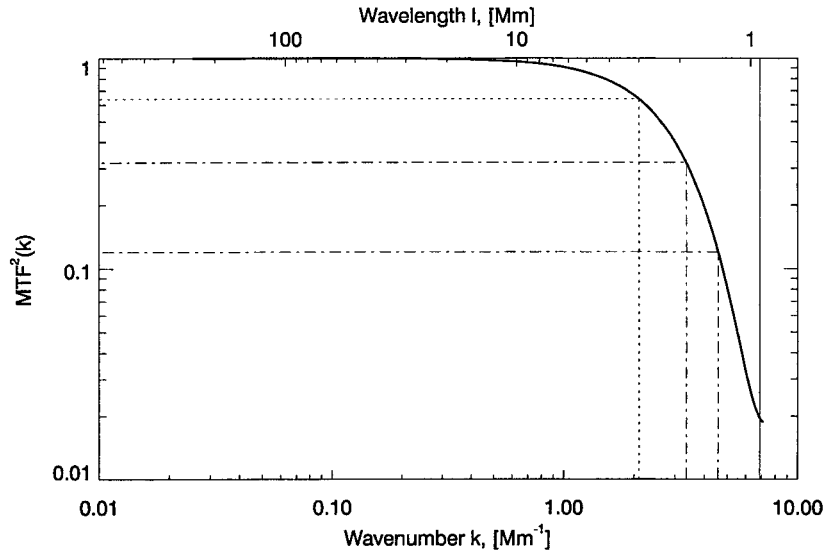


Figure 4. Modulation Transfer Function $MTF^2(k)$ for MDI data. $MTF^2(k) \approx 0.02$ at wave number $k_r = 6.88 \text{ Mm}^{-1}$, which corresponds to the resolution limit of the telescope (thin vertical line).

$$\sigma = \frac{\theta}{\sqrt{-8 \ln \frac{3}{8}}} \approx \frac{\theta}{2.8}. \quad (11)$$

The power spectrum of function $h(x)$ defined by (10) gives an estimate of MTF^2 for the MDI telescope (Figure 4).

We used expression (9) to obtain a noise- and-resolution corrected spectrum (hereafter denoted as AR MDI/ M^C) and we plot it in Figure 6(b) with a thick line. One sees that the correction has substantially changed the spectrum only at high wave numbers. The linear interval has been significantly extended into the range of high wave numbers, however the slope of the spectra did not change after the correction.

Since we have obtained the noise- and resolution-corrected spectrum, we are able to calculate a correction function for BBSO data ($|CF|_{\text{BBSO}}^{-2}$) by dividing the MDI corrected spectrum by the BBSO noise-corrected spectrum:

$$|CF|_{\text{BBSO}}^{-2} = \frac{E_{\text{MDI}}(k)}{E_{\text{BBSO}}(k)}. \quad (12)$$

Strictly speaking, the function $|CF|_{\text{BBSO}}^{-2}$ can only be used to correct a magnetic power spectrum obtained from BBSO data acquired under the same conditions as the active region magnetogram.

The above mentioned noise and resolution corrections were applied to the quiet-region magnetic power spectra. The BBSO quiet-Sun spectrum was first corrected for noise, while the MDI spectrum underwent the noise and resolution corrections.

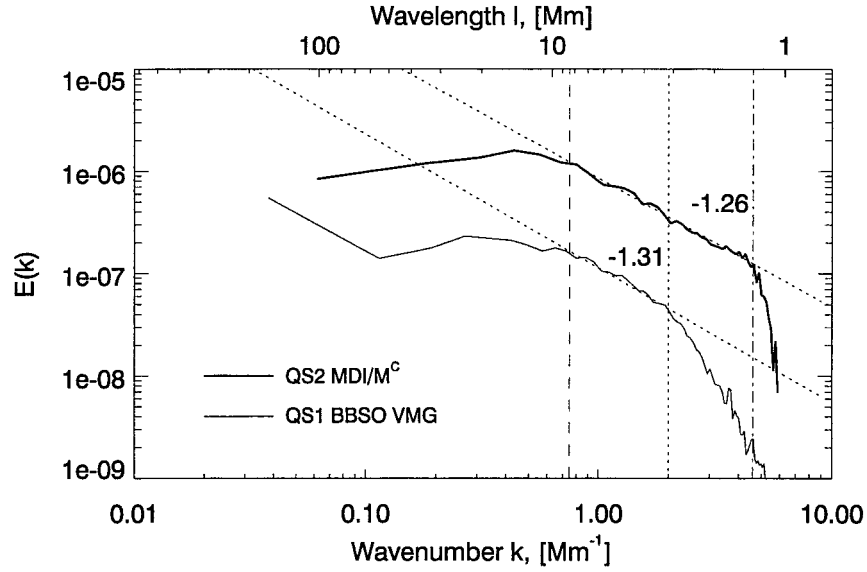


Figure 5. Quiet-region BBSO corrected power spectrum (QS1 BBSO VMG, *thin line*), and MDI power spectrum corrected with Modulation Transfer Function (QS2 MDI/M^C, *thick line*). The *dashed vertical* indicates the beginning of linear intervals on which power indices were defined. The *dotted vertical* shows the end of the linear interval in the QS1 BBSO VMG spectrum, while the *dash-dot line* indicates the end of the interval in the QS2 MDI/M^C spectrum.

Since the quality of the BBSO quiet-Sun and active-region magnetograms was approximately the same (only exposure time differs), we corrected the BBSO quiet-Sun spectrum with the correction function $|CF|_{\text{BBSO}}^{-2}$. Figure 5 shows the BBSO (thin lines, QS1 BBSO VMG) and MDI (thick lines, QS2 MDI/M^C) spectra. We used superscript ‘C’ to emphasize that both active- and quiet-region MDI magnetic power spectra were obtained by applying exactly the same correction routine.

4. The Spectra Analysis

In each corrected spectrum, we defined linear intervals and their slopes for three different ranges of wave numbers: low, intermediate and high wave numbers. The results are listed in Table I and represented in Figure 7. In the figure, the linear intervals are separated by spectral discontinuities (breaks in a spectrum).

One can see in Figures 6 and 7 that in ranges of low ($k < 0.6$) and intermediate wave numbers the active-region power spectra show fairly similar spectral behavior. In the intermediate range, the slopes of all the active region spectra are nearly the same and equal to -1.7 , while in the low-wave-number range the spectra behave as $\sim k^{-0.7}$. In Figure 6 we also see that including the sunspot in the calculation we extend the linear intermediate range far into large spatial scales (up to $l = 40$ Mm) without noticeable changes of a spectral slope, which is very similar

TABLE I

Linear intervals and spectral indices of the spectra. Notations $l_1(k_1)$ correspond to the beginning of a given linear interval and $l_2(k_2)$ to the end.

Spectrum	l_1 (Mm)	l_2 (Mm)	k_1 (Mm^{-1})	k_2 (Mm^{-1})	μ
Low-wave-number interval					
AR MDI/M ^C	127.5 ± 2.7	13.4 ± 3.6	0.049 ± 0.005	0.49 ± 0.13	-0.69 ± 0.03
AR MDI/M	127.5 ± 2.7	13.4 ± 3.6	0.049 ± 0.005	0.49 ± 0.13	-0.69 ± 0.03
AR BBSO VMG	127.5 ± 2.7	13.4 ± 3.6	0.049 ± 0.005	0.49 ± 0.13	-0.74 ± 0.08
QS2 MDI/M ^C	101.6 ± 3.1	14.5 ± 1.1	0.062 ± 0.006	0.43 ± 0.05	0.32 ± 0.02
QS1 BBSO VMG	54.9 ± 3.3	18.9 ± 4.3	0.114 ± 0.008	0.34 ± 0.08	0.49 ± 0.10
Intermediate-wave-number interval					
AR MDI/M ^C	8.0 ± 0.6	1.89 ± 0.20	0.78 ± 0.07	3.35 ± 0.36	-1.74 ± 0.06
AR MDI/M	8.1 ± 0.5	2.99 ± 0.19	0.77 ± 0.05	2.10 ± 0.13	-1.67 ± 0.04
AR BBSO VMG	11.0 ± 2.5	4.40 ± 0.25	0.59 ± 0.13	1.43 ± 0.08	-1.72 ± 0.15
QS2 MDI/M ^C	8.2 ± 0.7	1.38 ± 0.05	0.77 ± 0.06	4.57 ± 0.16	-1.26 ± 0.02
QS1 BBSO VMG	8.8 ± 1.2	3.17 ± 0.07	0.72 ± 0.11	1.98 ± 0.04	-1.31 ± 0.07
High-wave-number interval					
AR MDI/M ^C	1.48 ± 0.02	1.17 ± 0.02	4.25 ± 0.05	5.37 ± 0.10	-6.37 ± 0.13
AR MDI/M	2.87 ± 0.17	1.36 ± 0.10	2.20 ± 0.13	4.62 ± 0.34	-3.00 ± 0.15
AR BBSO VMG	3.60 ± 0.19	1.65 ± 0.17	1.74 ± 0.09	3.84 ± 0.37	-4.35 ± 0.08
QS2 MDI/M ^C	1.37 ± 0.02	1.10 ± 0.03	4.57 ± 0.07	5.68 ± 0.16	-8.12 ± 0.54
QS1 BBSO VMG	2.77 ± 0.12	1.74 ± 0.31	2.27 ± 0.09	3.70 ± 0.68	-3.88 ± 0.11

to Kolmogorov's spectrum $k^{-5/3}$. In the range of high wave numbers (Figure 7), all the active-region spectra behave differently and there is a tendency for a spectrum to be steeper with increasing of quality of the data.

The position of the spectral discontinuity between the low and intermediate ranges (low-wave-number break) in all the spectra is approximately the same and corresponds to scales of 8–12 Mm (Figure 7, see also Muller, 1988). This break appears, apparently, because we lack large-scale magnetic structures in the magnetograms.

The overall spectral behavior of the quiet-region spectra is very similar to that of the active-region spectra. There also are three spectral intervals in which the spectra have different slopes: $\mu \approx 0.4$ in the low-wave-number range and $\mu \approx -1.3$ in the intermediate range. At higher wave numbers the quiet-Sun spectra become steeper and, once again, we see that the better the resolution the steeper the spectrum.

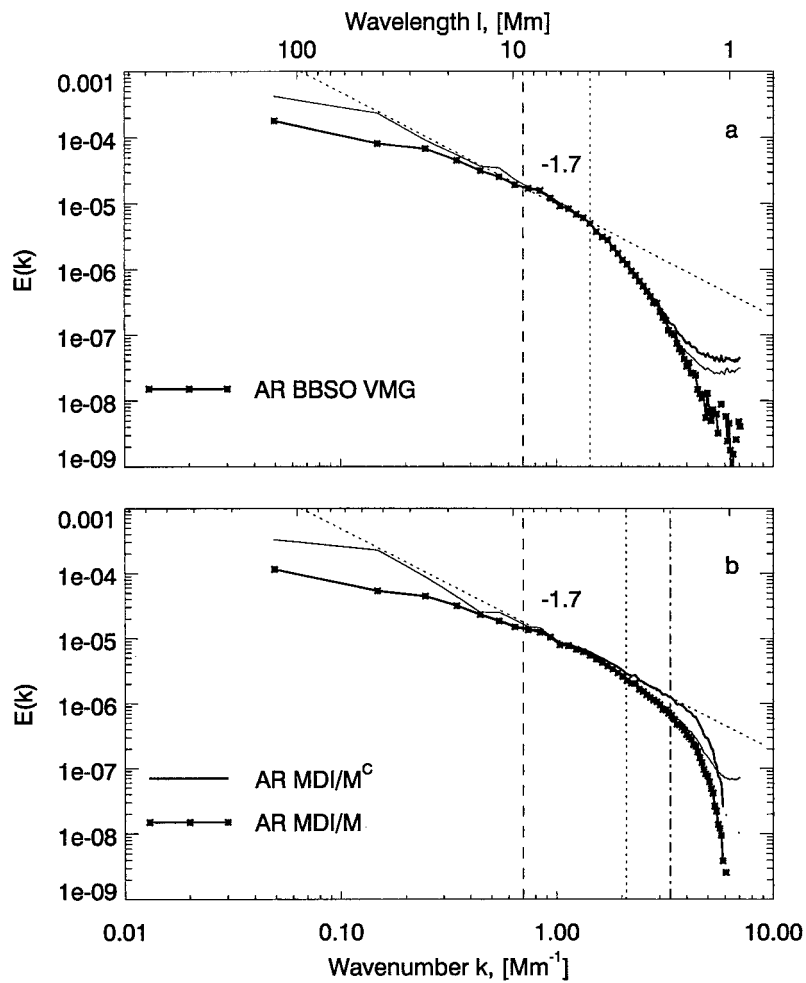


Figure 6. Top panel: BBSO active region power spectra: raw spectrum (*thin line*), ‘spot-corrected’ spectrum (*thick line*) and spot- and noise-corrected spectrum (*thick line with stars*). Bottom panel: MDI active region power spectra: raw spectrum (*thin line*), spot- and noise-corrected spectrum (AR MDI/M, *thick line with stars*) and spectrum corrected with MTF (AR MDI/M^C, *thick line*). The vertical lines indicate the beginning and the end of the linear intervals on which power indices were defined.

The high-wave-number break in the spectra between the intermediate and high-wave-number ranges deserves special attention. Unlike the low-wave-number break, the position of the high-wave-number break is not stable in k -space and it occurs at higher wave numbers as the data quality improves (see Figure 7).

We compare our spectra with previous results by Nakagawa and Priest (1973) and Lee *et al.* (1997). In Figure 8, we show three quiet-region power spectra calculated from observational data obtained with different instruments, seeing conditions and spatial resolution. For each spectrum, we define the ratio between wave

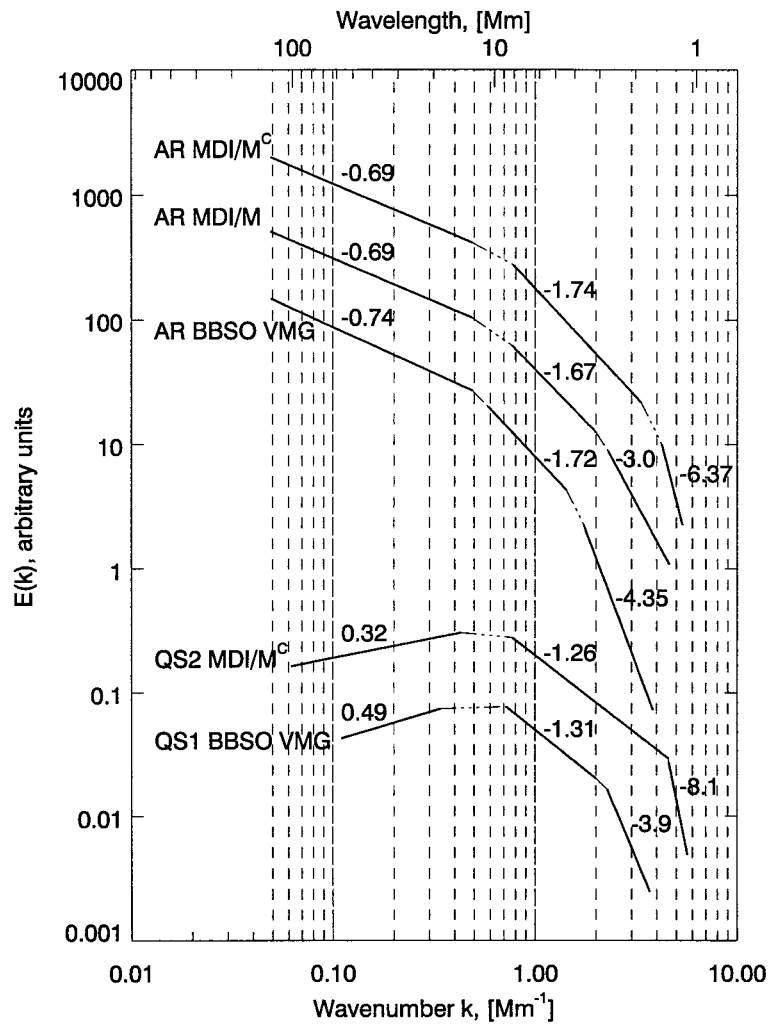


Figure 7. A schematic representation of all the magnetic power spectra obtained in the present study.

number k_r , which corresponds to the resolution limit of observational data and wave number k^* , where the high-wave-number break appears in a spectrum.

Nakagawa and Priest presented an uncorrected magnetic power spectrum with the high-wave-number break at $k^* = 0.63$ (spectra, denoted as NP 1973 in the figure). The spectrum was obtained from the Kitt Peak longitudinal magnetogram with spatial resolution of $5.0''$, which corresponds to $k_r = 1.73 \text{ Mm}^{-1}$ (note, that here $k = 2\pi/l$). For this spectrum we find the ratio $k_r/k^* = 2.75$. Lee *et al.* (1997) reported a high-wave-number break at $k^* = 3.0 \text{ Mm}^{-1}$ in the MTF-corrected spectrum obtained from BBSO data with spatial resolution of about $1.8''$ ($k_r = 4.9 \text{ Mm}^{-1}$). These values give the ratio k_r/k^* of 1.63 (the spectrum, denoted as Lee *et al.* in Figure 8). In the present paper, for the MDI quiet-region corrected

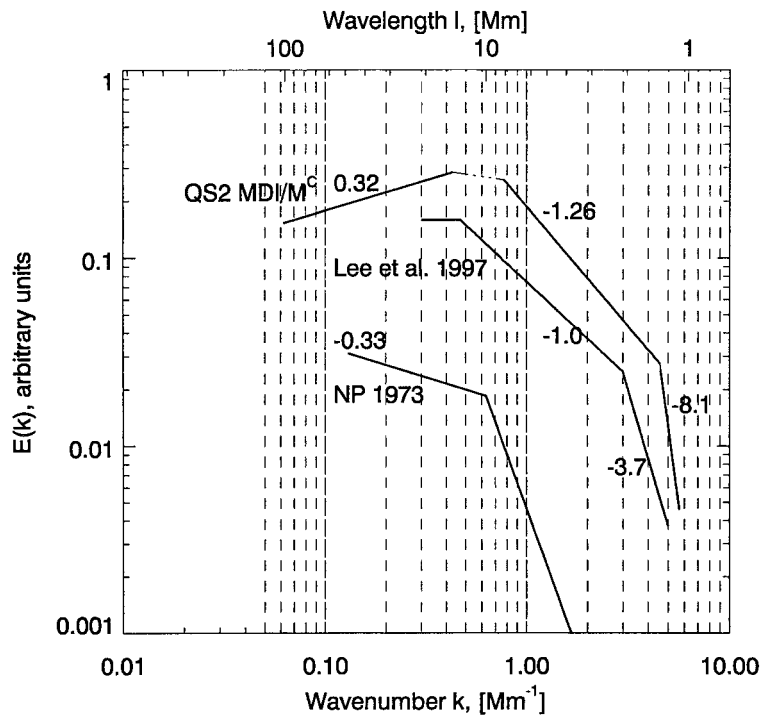


Figure 8. A schematic representation of the quiet-region MDI magnetic power spectra obtained in the present study and quiet-region magnetic power spectra calculated in previous works by Nakagawa and Priest (denoted in the figure as NP 1973) and by Lee and co-authors (denoted in the figure as Lee *et al.*, 1997).

spectrum (QS2 MDI/M^C in Figure 8) we find the ratio $k_r/k^* = 6.88/4.57 = 1.50$, where $k_r = 6.88 \text{ Mm}^{-1}$ corresponds to the diffraction limit of the MDI telescope, $1.25''$.

We also defined the ratio for the active-region spectra (see Figure 7). For the raw BBSO active-region spectrum the ratio $k_r/k^* = 4.33/1.43 = 3.03$ is defined by the $2''$ atmospheric limit of the resolution. For the raw MDI active-region spectrum the ratio is $k_r/k^* = 6.88/2.10 = 3.28$, and it decreased to $k_r/k^* = 6.88/3.35 = 2.10$ for the corrected spectrum (AR MDI/M^C in Figure 8).

One sees that the high-wave-number break is largely defined by the spatial resolution of the data, and it appears at higher wave numbers as the resolution of the data improves. In the case of the raw spectra, the break is positioned at wave numbers of about 3 times smaller than the wave number corresponding to the resolution of the data, and 1.5–2.0 times smaller in the case of the corrected spectra.

5. Conclusions and Discussion

(1) Using high-resolution MDI measurements of the photospheric magnetic fields we have obtained, for the first time, reliable magnetic power spectra in the high-wave-number range up to $k = 4.6 \text{ Mm}^{-1}$ that corresponds to spatial scale $l = 1.4 \text{ Mm}$.

(2) The power spectra for active- and quiet-region magnetic fields differ considerably and can be described as $\sim k^{-1.7}$ for the active-region magnetic field and as $\sim k^{-1.3}$ for the quiet-region field.

(3) The spectral behavior of the magnetic power spectra derived from the ground- and space-based measurements is substantially the same in the inertial intervals that changes according to spatial resolution of the data.

(4) We find that the spectral discontinuity (break) at high wave numbers is largely determined by the spatial resolution of the data and it appears at higher wave numbers as the resolution of the data improves. A correction of the raw magnetic power spectra extends the inertial range, while the spectral behavior on the inertial range remains the same. The break in the raw spectra is located at wave numbers about 3 times smaller than the wave number corresponding to the resolution limit of the data, and about 2.0-1.5 times smaller in the case of the noise- and resolution-corrected spectra.

It has been known that the magnetic power spectrum, like the velocity power spectrum, shows a spectral discontinuity at wave number $k \approx 3.0 \text{ Mm}^{-1}$ (Lee *et al.*, 1997, and references therein). The spectral discontinuity was interpreted to be the manifestation of the granular structure in the magnetic field pattern, and it represents distinct scale of spectral energy transfer (Muller, 1988; Lee *et al.*, 1997; Lawrence, Cadavid, and Ruzmaikin, 1999). On the other hand, our results indicate that the wave number $k = 3.0 \text{ Mm}^{-1}$ is not a special scale, and the magnetic power spectra with a slope of $\sim k^\mu$ may be extended into the high-wave-number range far beyond the limit of the spatial resolution of the present-day measurements. In other words, using the existing measurements of the magnetic fields, we do not reach the spatial scales where dissipative processes become significant. There is the expectation that increasingly improving observational technique will allow us to track down magnetic flux tubes that are much smaller in diameter than the highest spatial scale $l = 1.4 \text{ Mm}$ we obtained here. In Figure 9, under the assumption that the spectra may continue far into the high-wave-number range, we extended the active- and quiet-regions MDI spectra. One sees that they cross at spatial scale $l = 0.04 \text{ Mm}$. What is interesting about it is that this spatial scale is referred to as the smallest size of the magnetic flux tube in the solar photosphere (Schmieder *et al.*, 1996; Parker and Thyagaraja, 1999; Lin and Rimmele, 1999).

The main assumption of Kolmogorov's theory is that in fully developed isotropic turbulence, the driving force is acting only on large scales L and there are essentially no contribution coming from wave numbers larger than L^{-1} (Frisch, 1995). In this case, kinetic energy cascades from large to small spatial scales showing

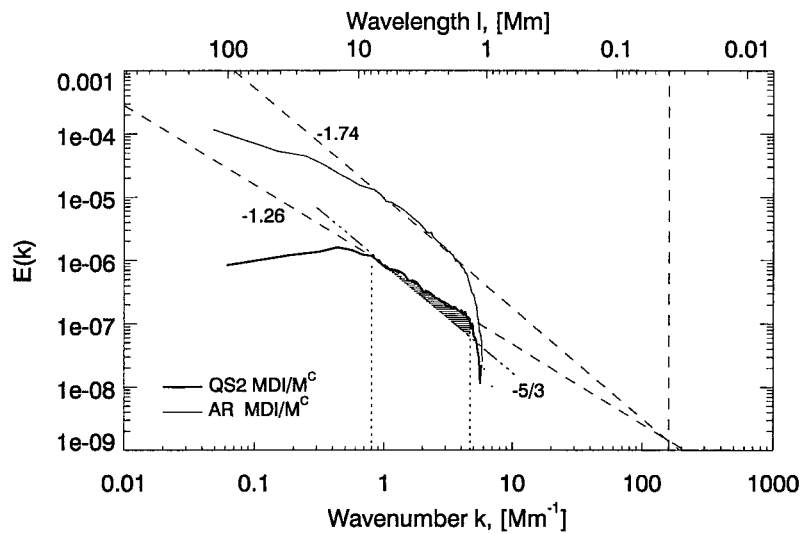


Figure 9. The active region (AR MDI/M^C, *thin line*) and quiet region (QS2 MDI/M^C, *thick line*) MDI corrected power spectra. *Dashed lines* show the best linear fit to the spectra in the inertial ranges. They cross each other at a spatial scale of about 40 km. The *shaded area* between the $-\frac{5}{3}$ line and the -1.26 dashed line corresponds to the lower limit of magnetic power apparently generated by small-scale dynamo action in the quiet-Sun photosphere.

spectral behavior with a power index of $-\frac{5}{3}$. We showed that the power spectrum for the quiet-region magnetic fields is considerably less steep and has the power-law index of -1.3 . If we assume that local small-scale dynamo operates in quiet-Sun region (Petrovay and Szakály, 1993; Cattaneo, 1999), then the additional energy brought by the dynamo will be redistributed along the spectrum (Monin and Yaglom, 1975) and this will decrease the value of the power-law index. We estimate the lowest relative amount of power generated by the small-scale dynamo under the assumption that the dynamo does not affect the magnetic power spectrum at wave numbers smaller than $L^{-1} = 0.77 \text{ Mm}^{-1}$. Total observed magnetic power in the inertial range was calculated as the area confined by the line $\sim k^{-1.26}$ on the top, and zero power level on the bottom, and the verticals $k = 0.77$ and $k = 4.57$ (see Figure 9). The shaded area in Figure 9 between the lines $-\frac{5}{3}$ and -1.26 within the inertial range $0.77 < k < 4.57$ can be treated as additional power generated by the small-scale dynamo action. The additional power is about 6.4% of the total observed magnetic power in the inertial range. As we have shown in this paper, the magnetic power spectrum with a slope of $\sim k^\mu$ may be extended into high-wave-numbers range. According to the latest estimations (Schmieder *et al.*, 1996; Parker and Thyagaraja, 1999; Lin and Rimmele, 1999), the magnetic flux tube can be as small as 50 km, which implies that more than 6% of magnetic energy may be generated by the small-scale dynamo.

Numerical modeling of turbulent convection showed that up to 20% of magnetic energy can be generated by solar granulation and supergranulation by means of the

local small-scale dynamo acting in the photosphere (Cattaneo, 1999). If Cattaneo is correct then the inertial range in the quiet-region magnetic power spectrum (see Figure 9) should end at spatial scales $l = 0.125 \text{ Mm}$ ($k = 0.77 \text{ Mm}^{-1}$). We expect that future improvement of the spatial resolution of the data will extend magnetic power spectra to much higher wave numbers, which will result in an increase of the estimated magnetic power generated by the small-scale dynamo.

The active-region magnetic power spectra are very close to Kolmogorov's spectrum with the power index of $-\frac{5}{3}$. A 44-hour sequence of MDI intensity images showed that the major part of the active-region magnetic fields was composed from the magnetic fields of the decaying sunspot. Magnetic flux was transported from the spot penumbra through the moat into the interior of the active region by turbulent photospheric plasma flows. This picture qualitatively corresponds to Kolmogorov's hypothesis on energy cascade, and may give us the reason that our active-region magnetic power spectrum is very close to Kolmogorov's spectrum.

Acknowledgements

This work was supported by NSF-ATM (97-14796) and NASA (NAG5-9682) grants. We thank M. Woodard and J. Lee for helpful discussions and comments. The authors also thank the anonymous referee for critical comments and suggestions. V.A. is grateful to Prof. P. Goode for the opportunity to work in the Big Bear Solar Observatory and to the staff of the BBSO for their warm hospitality and support.

References

- Cattaneo, F.: 1999, *Astrophys. J.* **515**, L39.
 Frisch, U.: 1995, *Turbulence, The Legacy of A.N. Kolmogorov*, Cambridge University Press, Cambridge.
 Knobloch, E. and Rosner, R.: 1981, *Astrophys. J.* **247**, 300.
 Lawrence, J.K., Cadavid, A.C., and Ruzmaikin, A.A.: 1999, *Astrophys. J.* **513**, 506.
 Lee, J.W., Chae, J.C., Yun, H.S., and Zirin, H.: 1997, *Solar Phys.* **171**, 269.
 Leighton, R.B.: 1964, *Astrophys. J.* **140**, 1547.
 Lin, H. and Rimmele, T.: 1999, *Astrophys. J.* **514**, 448.
 Monin, A.S. and Yaglom, A.M.: 1975, in J. Lumley (ed.), *Statistical Fluid Mechanics*, Vol. 2, MIT Press, Cambridge, MA.
 Muller, R.: 1988, in R. Rutten and G. Severino (eds.), *Solar and Stellar Granulation*, NATO ASI Ser. C, **263**, 101.
 Nakagawa, Y. and Priest, E.R.: 1973, *Astrophys. J.* **179**, 949.
 Nakagawa, Y. and Levine, R.H.: 1974, *Astrophys. J.* **190**, 441.
 Parker, E.N. and Thyagaraja, A.: 1999, *Solar Phys.* **189**, 45.
 Petrovay, K. and Szakaly, G.: 1993, *Astron. Astrophys.* **274**, 543.
 Schmieder, B., Rovira, M., Simnett, G. M., Fontenla, J. M., and Tandberg-Hanssen, E.: 1996, *Astron. Astrophys.* **308**, 957.
 Simon, G.W. and Leighton, R.B.: 1964, *Astrophys. J.* **140**, 1120.
 Wang, J.X., Wang, H., Tang, F., Lee, J.W., and Zirin, H.: 1995, *Solar Phys.* **160**, 277.